A Numerical Study of the Exact Evolution Equations for Surface Waves in Water of Finite Depth

By Yi A. Li, James M. Hyman, and Wooyoung Choi

We describe a pseudo-spectral numerical method to solve the systems of one-dimensional evolution equations for free surface waves in a homogeneous layer of an ideal fluid. We use the method to solve a system of one-dimensional integro-differential equations, first proposed by Ovsjannikov and later derived by Dyachenko, Zakharov, and Kuznetsov, to simulate the exact evolution of nonlinear free surface waves governed by the two-dimensional Euler equations. These equations are written in the transformed plane where the free surface is mapped onto a flat surface and do not require the common assumption that the waves have small amplitude used in deriving the weakly nonlinear Korteweg–de Vries and Boussinesq long-wave equations. We compare the solution of the exact reduced equations with these weakly nonlinear long-wave models and with the nonlinear long-wave equations of Su and Gardner that do not assume the waves have small amplitude. The Su and Gardner solutions are in remarkably close agreement with the exact Euler solutions for large amplitude solitary wave interactions while the interactions of low-amplitude solitary waves of all four models agree. The simulations demonstrate that our method is an efficient and accurate approach to integrate all of these equations and conserves the mass, momentum, and energy of the Euler equations over very long simulations.

Address for correspondence: Wooyoung Choi, Department of Naval Architecture and Marine Engineering, University of Michigan, Ann Arbor, MI 48109; e-mail: wychoi@engin.umich.edu

STUDIES IN APPLIED MATHEMATICS 113:303–324

Published by Blackwell Publishing, 350 Main Street, Malden, MA 02148, USA, and 9600 Garsington Road, Oxford, OX4 2DQ, UK.

1. Introduction

In this paper, we fully model the nonlinear surface waves by solving a system of two one-dimensional evolution equations derived from the two-dimensional Euler equations for the free surface elevation and the velocity potential on the parameterized free surface. These integral–partial differential equations are then accurately solved using a fast Fourier transform (FFT) pseudo-spectral numerical method.

The discrete Fourier series and the boundary integral methods are widely used numerical methods to fully model the nonlinear water wave dynamics governed by the Euler equations for ideal fluids. See a review by Tsai and Yue [1] of various numerical methods for water wave problems.

Earlier Fenton and Rienecker [2] expressed the free surface elevation and the velocity potential as Fourier series in space and integrated the Euler equations using the FFT for spatial derivatives and a leap-frog scheme for time evolution. However, this formulation is inconvenient for evaluating the vertical velocity at the free surface when imposing the nonlinear free surface boundary conditions. Dommermuth and Yue [3] improved the efficiency of the method by expanding the vertical velocity at the free surface about the undisturbed (flat) free surface. A slightly different formulation, proposed by Craig and Sulem [4], expressed the formal solution of the Euler equations in terms of the Dirichlet-Neumann operator and approximated the vertical velocity by expanding the operator in powers of the surface elevation.

The boundary integral method parameterizes the free surface using Lagrangian coordinates and, by applying Green's theorem, the velocity potential is expressed in terms of a distribution of singularities on the free surface, whose strengths have to be determined [5]. Thus, although the boundary integral formulation solves some of the difficulties in imposing the free surface boundary conditions that the Fourier series approach encounters, it requires accurate approximations of the singular integrals along the free surface.

Both approaches can accurately simulate the surface waves before the waves break but they are numerically complex to implement. Here, we solve the system of one-dimensional integro-differential equations, proposed by Ovsjannikov [6] and derived explicitly by Dyachenko, Zakharov, and Kuznetsov [7] using the time-dependent conformal mapping technique to map the fluid region of interest to a strip. Their one-dimensional system of integro-differential equations is an *exact and closed* system for fully nonlinear free surface waves in a homogeneous layer of an ideal fluid described by the two-dimensional Euler equations. This idea was further generalized and tested by Choi and Camassa [8] for periodic traveling gravity waves. Unlike the boundary integral method, this approach does not require approximating complicated singular integrals and extra steps to compute the strengths of singularities, and can be solved accurately using an FFT pseudo-spectral method. Compared with the

previous pseudo-spectral methods proposed by Dommermuth and Yue [3] and Craig and Sulem [4], the equations are written in the transformed plane where the free surface is mapped onto a flat surface and do not require an expansion assuming that the waves have small amplitude.

Because the full Euler equations are often too complicated to analyze directly, simpler models are commonly used to gain physical insight into the dynamics of nonlinear waves. See, for example, Choi [9] for various asymptotic models for water waves. Small-amplitude, long-wavelength waves are often approximated by weakly nonlinear long-wave models such as the Korteweg–de Vries (KdV) and the Boussinesq equations [10, 11]. Relaxing the assumption that waves have small amplitude, Su and Gardner [12] derived the higher-order nonlinear long-wave model. As the model of Su and Gardner requires no assumption on wave amplitude, it is expected to better approximate the exact evolution equations than the classical weakly nonlinear models, but this has not been carefully examined.

After describing our numerical method for solving the exact evolution equations, we briefly review the approximate models and describe their relationships. We then demonstrate the effectiveness of our numerical method in simulations of solitary wave collisions in water of finite depth and compare numerical solutions of the exact system with those of various asymptotic models for long waves. The interactions of low-amplitude solitary waves for all of the long-wave models are in close agreement, even beyond the weakly nonlinear regime. When the waves have high amplitude, then only the Su and Gardner solutions are close to the solutions of the full Euler equations.

2. Mathematical formulation

A two-dimensional ideal flow between the free surface at $y = \zeta(x, t)$ and the flat bottom at $y = -h$ is governed by the Euler equations. These equations can be expressed in terms of the velocity potential $\Phi(x, y, t)$ as

$$\begin{aligned}
&\Phi_{xx} + \Phi_{yy} = 0, && -h < y < \zeta,\ -\infty < x < \infty,\\
&\Phi_y = \zeta_t + \Phi_x \zeta_x, && -\infty < x < \infty,\ y = \zeta(x, t),\\
&\Phi_t + \tfrac{1}{2}|\nabla\Phi|^2 + gy = \sigma \zeta_{xx} \big/ \left(1 + \zeta_x^2\right)^{3/2} + \mathcal{P}_{\mathrm{E}}/\rho, && -\infty < x < \infty,\ y = \zeta(x, t),\\
&\Phi_y = 0, && -\infty < x < \infty,\ y = -h,
\end{aligned} \tag{1}$$

where ρ is the fluid density, σ is the surface tension, and $\mathcal{P}_{\mathrm{E}}(x, t)$ is a prescribed external pressure.

2.1. Derivation of exact evolution equations

Following the work by Dyachenko et al. [7] and Choi and Camassa [8], let $z(\xi, \eta, t) = x(\xi, \eta, t) + iy(\xi, \eta, t)$ be an analytic function in the horizontal

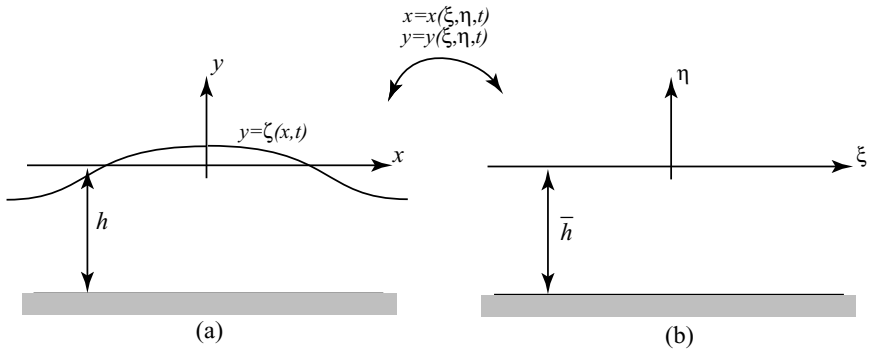

Figure 1. Conformal mapping between (a) physical domain (x, y) and (b) mathematical domain (ξ, η).

strip $-\bar{h} \le \eta \le 0$, where $z - \xi$ is periodic in ξ with period l, such that $z(\xi, \eta, t)$ maps the rectangle of $-l/2 \le \xi \le l/2$, $-\bar{h} \le \eta \le 0$ onto the fluid domain (see Figure 1). The mapping function satisfies $y(\xi, 0, t) = \zeta(x(\xi, 0, t), t)$ and $y(\xi, -\bar{h}, t) = -h$ for any $\xi \in [-l/2, l/2]$.

It follows from the Cauchy–Riemann equations that the parameterized functions $x(\xi, \eta, t)$, $y(\xi, \eta, t)$, $\phi(\xi, \eta, t) = \Phi(x(\xi, \eta, t), y(\xi, \eta, t), t)$ and its harmonic conjugate $\psi(\xi, \eta, t)$ are related by the Fourier multiplier transforms [8]. That is, if the Fourier series of $y(\xi, 0, t)$ and $\psi(\xi, 0, t)$ are given by

$$y(\xi, 0, t) = a_0 + \sum_{k=1}^{\infty} \left(a_k e^{-2\pi i k\xi/l} + \mathrm{CC} \right),$$

$$\psi(\xi, 0, t) = b_0 + \sum_{k=1}^{\infty} \left(b_k e^{-2\pi i k\xi/l} + \mathrm{CC} \right),$$

then, for any $\eta \in [-\bar{h}, 0]$, the following relations hold

$$\begin{aligned}
y(\xi, \eta, t) &= \frac{a_0 + h}{\bar{h}}\eta + a_0 + \sum_{k=1}^{\infty} \left[S_k(\eta) a_k e^{-2\pi i k\xi/l} + \mathrm{CC} \right], \\
\psi(\xi, \eta, t) &= \frac{b_0}{\bar{h}}\eta + b_0 + \sum_{k=1}^{\infty} \left[S_k(\eta) b_k e^{-2\pi i k\xi/l} + \mathrm{CC} \right], \\
x(\xi, \eta, t) &= \frac{a_0 + h}{\bar{h}}\xi + x_0 + \sum_{k=1}^{\infty} \left[i C_k(\eta) a_k e^{-2\pi i k\xi/l} + \mathrm{CC} \right], \\
\phi(\xi, \eta, t) &= \frac{\alpha_0}{\bar{h}}\xi + \phi_0 + \sum_{k=1}^{\infty} \left[i C_k(\eta) b_k e^{-2\pi i k\xi/l} + \mathrm{CC} \right],
\end{aligned} \tag{2}$$

where CC represents the complex conjugate, a_0 and b_0 are real, a_k and b_k are complex, and

$$S_k(\eta) = \sinh[2\pi k(\eta + \bar{h})/l]/\sinh(2\pi k\bar{h}/l),$$

$$C_k(\eta) = \cosh[2\pi k(\eta + \bar{h})/l]/\sinh(2\pi k\bar{h}/l).$$

As the time derivatives of x and ϕ in (2) must be periodic in ξ for periodic waves, the coefficients of the linear functions in ξ have to be independent of time. This is accomplished by choosing $\bar{h}$ and b_0 as $\bar{h}(t) = a_0(t) + h$ and $b_0(t) = c\bar{h}(t)$, where constant c is determined from the initial condition.

On the free surface at $\eta = 0$, (2) gives the following relations:

$$x_\xi = 1 - T[y_\xi], \quad \phi_\xi = c - T[\psi_\xi], \tag{3}$$

where all variables are evaluated at $\eta = 0$, and T is the Fourier multiplier operator defined by

$$\begin{aligned} T[y] &= \frac{1}{2\bar{h}} \int_{-\infty}^{\infty} y(\xi', 0, t) \coth\left[\frac{\pi}{2\bar{h}}(\xi' - \xi)\right] d\xi' \\ &= \sum_{k=1}^{\infty} \left[-i \coth(2\pi k\bar{h}/l) a_k e^{-2\pi i k\xi/l} + \mathrm{CC}\right], \end{aligned} \tag{4}$$

which we call the T-transform.

For deep water ($h \to \infty$), The T-transform becomes the Hilbert transformation H defined by

$$H[y] = \int_{-\infty}^{\infty} \frac{y(\xi', 0, t)}{\xi' - \xi}\, d\xi' = \sum_{k=1}^{\infty} \left[-i a_k e^{-2\pi i k\xi/l} + \mathrm{CC}\right]. \tag{5}$$

Integrating (3) once with respect to ξ yields

$$x(\xi, 0, t) = \xi + x_0 - T[y], \quad \phi(\xi, 0, t) = c\xi + \phi_0 - T[\psi], \tag{6}$$

where y and ψ are also evaluated at $\eta = 0$, and x_0, and ϕ_0 are functions of time to be determined.

By substituting the expressions for x, y, ϕ and ψ at $\eta = 0$ into the free surface boundary conditions in (1), we obtain the *surface Euler equations* [8] for $x(\xi, 0, t)$, $y(\xi, 0, t)$, and $\phi(\xi, 0, t)$:

$$\begin{aligned} x_t &= x_\xi T\left[\frac{\psi_\xi}{J}\right] + y_\xi \left(\frac{\psi_\xi}{J}\right), \\ y_t &= -x_\xi \left(\frac{\psi_\xi}{J}\right) + y_\xi T\left[\frac{\psi_\xi}{J}\right], \\ \phi_t &- \phi_\xi T\left[\frac{\psi_\xi}{J}\right] + \frac{1}{2J}(\phi_\xi^2 - \psi_\xi^2) + gy = \frac{\sigma(y_{\xi\xi}x_\xi - y_\xi x_{\xi\xi})}{J^{3/2}} - \frac{\mathcal{P}_\mathrm{E}}{\rho}, \end{aligned} \tag{7}$$

where $J = x_\xi^2 + y_\xi^2$ and $\psi(\xi, 0, t)$ is related to $\phi(\xi, 0, t)$ from (6). From now on, the dependence on η in x, y, ϕ, and ψ will be dropped, since only the variables evaluated at $\eta = 0$ appear in (7).

Because x and y are related by the Cauchy–Riemann equations, or (6), it is sufficient to solve one of the first two equations with the third equation in (7). We however found it convenient to numerically solve all these equations and determine both $x_0(t)$ and $a_0(t)$ from the first two equations.

Equation (7) is the exact parametric evolution equations for surface gravity–capillary waves under pressure forcing in water of finite depth. Notice that no assumptions have been made to derive (7) from (1). The formulation is similar to the boundary integral method for two-dimensional water wave problems where the evolution equations are written in terms of physical variables defined on the boundary and the dimension of the original problem is reduced by one. The nonlocal (linear) operator in the evolution equations can be easily evaluated by the pseudo-spectral method described in the subsequent section.

2.2. Numerical method

At each time step, the periodic functions (x, y, ϕ, ψ) are expanded as discrete Fourier series in ξ using the FFT and their derivatives and T-transform are computed in Fourier space. For example, the T-transform of a function can be found via FFT after multiplying the Fourier coefficients by $-i \coth(2\pi k\bar{h}/l)$, as shown in (4). With evaluating nonlinear terms in physical space, we advance the solution of (7) in time with a variable-order, variable-stepsize, Adams–Bashford–Moulton predictor–corrector method.

We use artificial dissipation (hyperviscosity) to reduce the aliasing error in solving nonlinear equations (7). The diffusive terms $\nu\Delta\xi x_{\xi\xi}$, $\nu\Delta\xi y_{\xi\xi}$, and $\nu\Delta\xi\phi_{\xi\xi}$ are evaluated, passed through a high-pass filter, and added to the right-hand side of the x, y, and ϕ equations, respectively. Here, $\Delta\xi$ is the spatial step size and ν is chosen in the range between 0.01 and 0.05. To preserve the accuracy in the lower frequency modes, a high-pass filter defined in the Fourier space eliminates the lowest 1/2 Fourier modes of the dissipation terms, leaves the highest 3/5 modes unchanged, and has the linear transition between the two regions. Thus, the dissipation has no direct effect on the lower 1/2 of the Fourier modes of the solution, and only dissipates the higher 1/2 modes.

In the absence of surface tension and atmospheric external pressure, the surface wave equations have nine one-parameter symmetry groups [13], from which eight conserved quantities can be found. The accuracy of our numerical solutions is monitored by the following three conserved quantities: conservation of mass

$$\int_{-l/2}^{l/2} y(\xi, t) x_\xi(\xi, t)\, d\xi,$$

conservation of horizontal momentum

$$\int_{-l/2}^{l/2} \phi_\xi(\xi, t) y(\xi, t)\, d\xi,$$

and conservation of energy

$$\int_{-l/2}^{l/2} \left(\phi_\xi(\xi, t)\psi(\xi, t) + g y(\xi, t)^2 x_\xi(\xi, t)\right) d\xi.$$

The spatial resolution is between 512 and 2048 Fourier modes based the steepness of the solution. The time step and spatial resolution are determined so that the absolute error of conserved quantities is below 10^{-4} and the relative error is below 10^{-3}.

2.3. Approximate models

Here, we briefly review the approximate evolution equations for long waves. In 1969, Su and Gardner [12] derived a system of equations under the sole assumption that a typical wavelength l is much greater than water depth h, in other words, $\epsilon(\equiv h/l) \ll 1$. The Su–Gardner (SG) system[1] is given, in terms of ζ and the depth-mean velocity $\bar{u}$, by

$$\begin{aligned} &\zeta_t + [(h+\zeta)\bar{u}]_x = 0, \\ &\bar{u}_t + \bar{u}\bar{u}_x + g\zeta_x = \frac{1}{3(h+\zeta)}\left[(h+\zeta)^3\left(\bar{u}_{xt} + \bar{u}\bar{u}_{xx} - \bar{u}_x^2\right)\right]_x. \end{aligned} \tag{8}$$

Notice that the first equation in (8) implying the conservation of mass is exact, while the second equation for conservation of momentum contains an absolute error of $O(\epsilon^4)$. Because no assumption that wave amplitude is small has been imposed to derive this model, the system of equations in (8) should be a good approximation of the Euler equations even for large amplitude waves, as long as the long-wave approximation ($\epsilon \ll 1$) is valid.

Under the same order of approximation, other forms of equations can be obtained using, instead of $\bar{u}$, a different velocity. For example, if the horizontal velocity is defined at a certain depth as $y = y_\alpha$, then the asymptotic relationship between $\bar{u}$ and $\tilde{u} \equiv u(x, y = y_\alpha, t)$ can be expressed as [15]

$$\bar{u} = \tilde{u} + \tfrac{1}{2}(h + y_\alpha)^2 \tilde{u}_{xx} - \tfrac{1}{6}(h+\zeta)^2 \tilde{u}_{xx} + O(\epsilon^4). \tag{9}$$

Substituting this into (8) results in the system derived by Wei et al. [16]. Their system is asymptotically equivalent to (8) but the two systems possess different linear dispersion relations and conservation laws.

[1]This system of equations is also called the Green–Naghdi (GN) equations [14].

Under the weakly nonlinear assumption that $\zeta/h = O(\epsilon^2)$ and $\bar{u}/(gh)^{1/2} = O(\epsilon^2)$, after dropping higher-order terms than $O(\epsilon^4)$, the strongly nonlinear system (8) becomes the Boussinesq equations

$$\begin{aligned} \zeta_t + [(h+\zeta)\bar{u}]_x &= 0, \\ \bar{u}_t + \bar{u}\bar{u}_x + g\zeta_x &= \frac{h^2}{3}\bar{u}_{xxt}. \end{aligned} \tag{10}$$

For uni-directional waves, these equations can be further reduced to the KdV equation

$$\zeta_t + c_0\zeta_x + \frac{3c_0}{2h}\zeta\zeta_x + \frac{c_0h^2}{6}\zeta_{xxx} = 0, \tag{11}$$

where $c_0 = \sqrt{gh}$.

The solitary wave solutions for the KdV equation (11) and the SG equations (8) are

$$\zeta_{\mathrm{KdV}} = \frac{2h(c-c_0)}{c_0}\,\mathrm{sech}^2\,\frac{\sqrt{3(c-c_0)}(x-ct)}{\sqrt{2c_0}h},$$

$$\zeta_{\mathrm{SG}} = \frac{c^2-c_0^2}{g}\,\mathrm{sech}^2\,\frac{\sqrt{3\left(c^2-c_0^2\right)}(x-ct)}{2ch},$$

respectively, for given wave speed c. The explicit solitary wave solutions for the Boussinesq equations are not known, and they must be calculated numerically.

3. Exact solitary wave solutions

We solve the surface Euler equations (7) for solitary waves of the Froude number up to $F = 1.27$ with 2048 discrete Fourier modes, using the modified Newton's method (as described in the Appendix). Beyond $F = 1.27$, the solitary wave requires more Fourier modes due to the steepening of wave slope. Because our objective is to investigate the dynamics of solitary waves (not to compute the highest solitary wave of $F \simeq 1.286$), we only consider solitary waves of $F < 1.27$.

In Figure 2, we compare solitary wave profiles of various models for three different Froude numbers $F = c/\sqrt{gh}$ =1.0838, 1.2012, and 1.2691. For the Froude number close to 1, solitary wave solutions of the KdV, Boussinesq, and SG equations are very close to those of the Euler equations, as expected. However, as F increases, solitary waves of the KdV equation are quite different from those of the Euler equations and, for given wave speed, the amplitude of the KdV solitary wave is much smaller than that of the Euler solitary wave. Solitary waves for the bi-directional SG and Boussinesq equations are slightly wider and narrower, respectively, than those for the Euler equations but show a

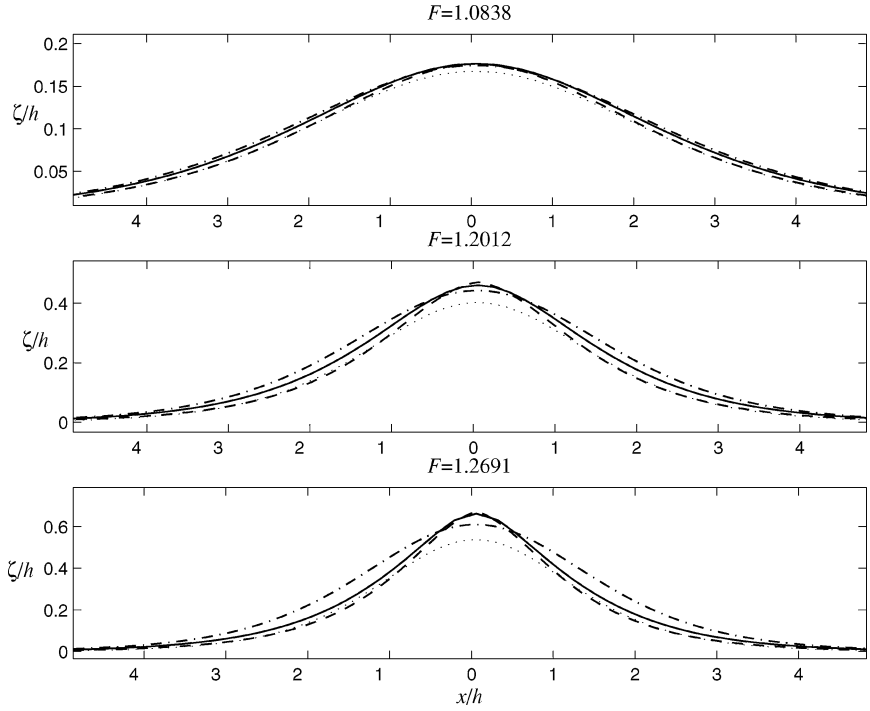

Figure 2. Solitary wave profiles at the Froude numbers of $F = 1.0838$, 1.2012, and 1.2691 for the Euler (solid curve), SG (dash-dotted curve), Boussinesq (dashed curve), and KdV (dotted curve) equations. Notice that the solitary wave solutions of the KdV, Boussinesq, and SG equations are very close to those of the Euler equations for Froude number close to 1. However, the solitary waves of the KdV equation are quite different from those of the Euler equations for larger Froude number.

little better agreement with the Euler solutions than what the KdV theory predicts.

For more quantitative comparisons, the scaled mass of solitary waves $M = \int_{\mathbb{R}} \eta \, dx/h^2$ and the scaled wave amplitude a/h as a function of the Froude number are shown in Figures 3 and 4. Notice that our numerical solutions for solitary waves for (7) agree well with the earlier results of Longuet-Higgins [17] and Longuet-Higgins and Fenton [18] and the maximum difference is 0.16% for M and 0.35% for a/h.

When the Froude number is close to 1 (say, $1 \leq F < 1.05$), all the solitary waves have almost the same mass, as shown in Figure 3. As F increases ($1.05 < F < 1.15$), the mass of solitary wave of the strongly nonlinear long-wave model (SG) is closer to that of the Euler wave than any other weakly nonlinear models. Because the derivation of the SG equations did not assume the wave amplitudes were small, it is not surprising that the SG equations are valid for relatively larger F than any weakly nonlinear models. When F further

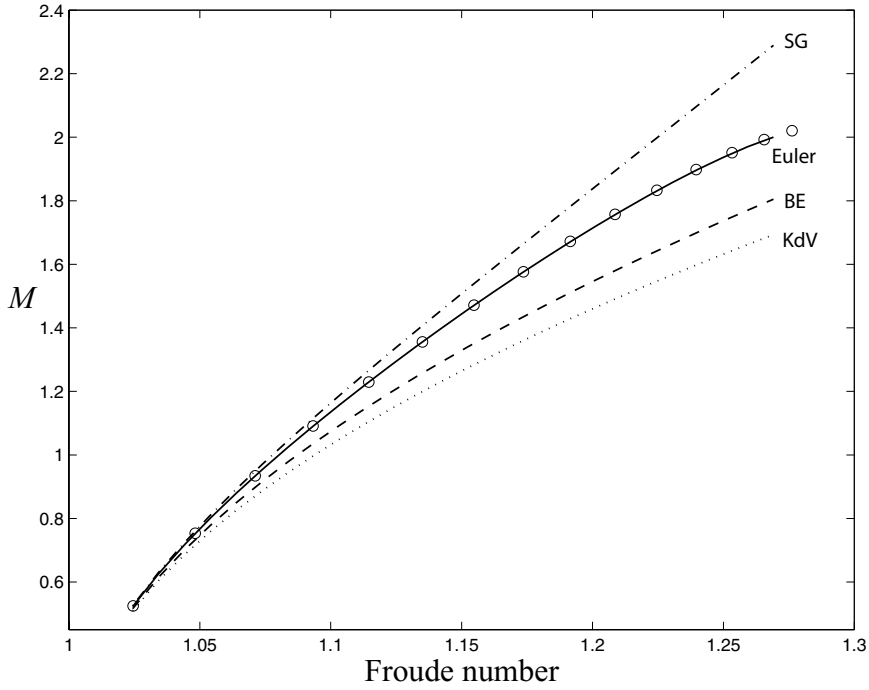

Figure 3. The solitary waves increases in height and mass M as a function of the Froude number F for the Euler (solid curve), SG (dash-dotted curve), Boussinesq (dashed curve), KdV (dotted curve), and Longuet-Higgins and Fenton (circle) models.

increases ($F > 1.15$), none of the approximate models are accurate and the fully nonlinear solutions of the Euler equations are required. It is well known [18] that exact solitary wave steepens as wave amplitude increases so that the slope at the crest becomes discontinuous at $F \approx 1.286$, violating the long-wave assumption, and therefore any long-wave models should be inapplicable for large F. Similar observations can be made from the relationship between wave amplitude and the Froude number, as shown in Figure 4.

4. Numerical simulations

We compare the numerical solutions of the exact evolution equations with those of approximate evolution equations to demonstrate the effectiveness of the numerical method on this class of equations. The examples also illustrate validity of the approximate long-wave models in head-on and overtaking collisions of solitary waves, as well as the disintegration of an elevation. These simulations add to the previous investigations of these approximate models using different approaches [19–23]. Throughout this section, time t is nondimensionalized by h/c_0.

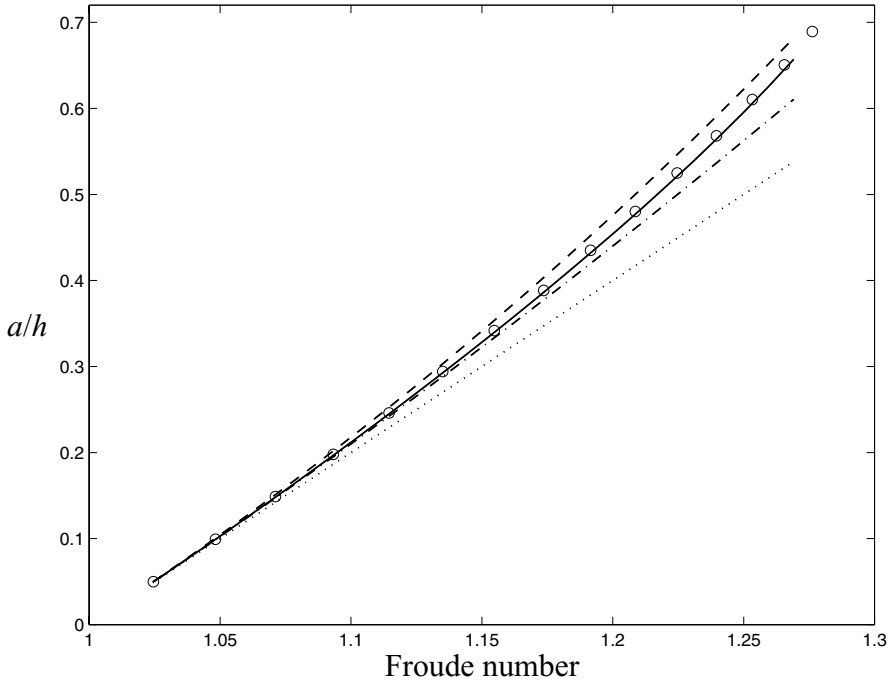

Figure 4. Wave amplitude (a/h) versus the Froude number (F): Euler (solid curve), SG (dash-dotted curve), Boussinesq (dashed curve), KdV (dotted curve), and Longuet-Higgins and Fenton (circle). Notice that the KdV solitary wave of given wave amplitude is moving much faster than the Euler solitary wave with the same amplitude.

4.1. Head-on collision of solitary waves

In the head-on collision shown in Figure 5, two solitary waves with $F = 1.172$ and 1.084 propagating in the opposite directions collide and re-emerge with oscillating tails. We match wave speeds, and thus wave amplitudes for different models are different, as discussed in Section 3. Initially, the amplitudes of the larger waves are $a_E/h = 0.3847$, $a_S/h = 0.3727$, and $a_B/h = 0.3991$ and those of the smaller waves are $a_E/h = 0.1765$, $a_S/h = 0.1744$, and $a_B/h = 0.1801$ for the Euler, Su–Gardner, and Boussinesq equations, respectively. Because the KdV model is for unidirectional waves, it is not included in this example. Notice that the amplitudes of the larger waves are not in the weakly nonlinear regime.

As shown in Figure 5, two solitary waves collide to form a single peak at $t = 25.9$ with amplitudes of $a_E/h = 0.5991$, $a_S/h = 0.5802$, and $a_B/h = 0.6052$. The height of the peak during the collision is always greater than the sum of two wave amplitudes. After the head-on collision, small dispersive waves are shed behind solitary waves and the amplitudes of both waves slightly decrease.

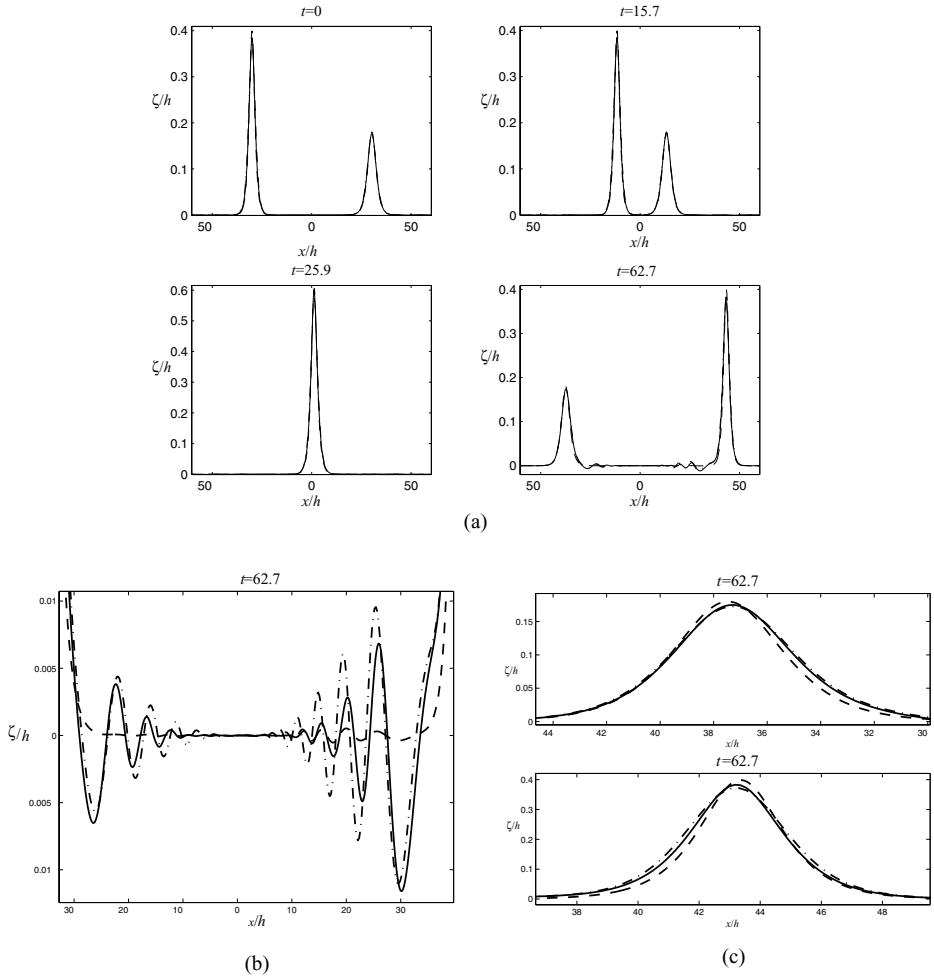

Figure 5. (a) The head-on collision of two solitary waves of the Euler equations (solid curve) is compared with numerical solutions of the SG equations (dash-dotted curve) and the Boussinesq equations (dashed curve), respectively, with the Froude numbers of $F = 1.084$ and 1.172. Two solitary waves collide to form a single peak greater than the sum of two wave amplitudes. (b) The trailing tails of solitary waves after the head-on collision. (c) The final solitary wave profiles after the head-on collision show that small-dispersive waves are shed behind solitary waves and the amplitudes of both waves slightly decrease.

The dispersive tails generated after the collision (enlarged in Figure 5(b)) show that the SG equations more accurately approximate the Euler equations than the Boussinesq equations in terms of wave amplitude and phase. As expected, our numerical results verify that solitary waves of these three systems are not true solitons, i.e., they do not maintain the same shape after interactions, and dispersive tails become larger as solitary wave amplitudes increase.

After the collision, both solitary waves are retarded from their own pathlines and this phase shift is known to be a salient feature of the nonlinear interaction of solitary waves. The decay of kinetic energy by the retardation upon merging is compensated for by the increase of potential energy, or the increase of the peak height [23]. For weakly nonlinear waves, the phase shift of one wave is known to be proportional to the square root of amplitude of the other wave. This phase shift is too small to be accurately measured in our numerical solutions, but the finite amplitude effect on the phase shift can be identified from the relative positions of different solitary waves. As shown in Figure 5(c), the weakly nonlinear model (Boussinesq equations) underpredicts the phase shift after the collision, while the phase shift for the SG equations is very close to that for the Euler equations.

The phase shift is more noticeable in the head-on collision of higher amplitude waves with $F = 1.172$ and 1.201, as shown in Figure 6. The differences in dispersive tails and phase shifts are greater in this highly nonlinear regime. The strong nonlinearity in the Euler and SG equations induces a larger phase shift.

In our numerical experiments, we match wave speeds by choosing different wave amplitudes for different models. When we use solitary waves of same amplitude for all models, the difference among various models will be even greater than the results shown here. From Figure 4, it is expected that the interaction of SG solitary waves will be closer to that of Euler solitary waves because the wave speed of the SG model is much closer to that of the Euler equations than any other models (up to intermediate wave amplitude). When we further increase wave amplitude, no asymptotic theory will be valid and fully nonlinear simulation is required.

4.2. Overtaking collision of solitary waves

For the overtaking collision of two KdV solitons, it is well known [15, 23] that, depending on the amplitude ratio, two waves can either remain separated or merge into a single peak during their interaction. From the weakly nonlinear analysis, the critical amplitude ratio is known to be 3 and the larger solitary wave overtaking the smaller one experiences a forward phase shift, while the smaller wave shifts backward.

Figure 7 shows the overtaking collision of two solitary waves with the Froude numbers of $F = 1.156$ and 1.09 in a frame moving with the speed $F = 1.123$. Initially, the amplitudes of the larger waves are $a_K/h = 0.3114$, $a_E/h = 0.3441$, $a_S/h = 0.3356$, and $a_B/h = 0.3561$, and the amplitudes of the smaller waves are $a_K/h = 0.1808$, $a_E/h = 0.1911$, $a_S/h = 0.1889$, and $a_B/h = 0.1952$ for the KdV, Euler, SG, and Boussinesq equations, respectively. With this amplitude ratio (about 1.8), two waves never merge into a single peak.

Unlike the case of head-on collision, the overtaking collision of solitary waves of all models are nearly elastic (except the KdV equation, for which

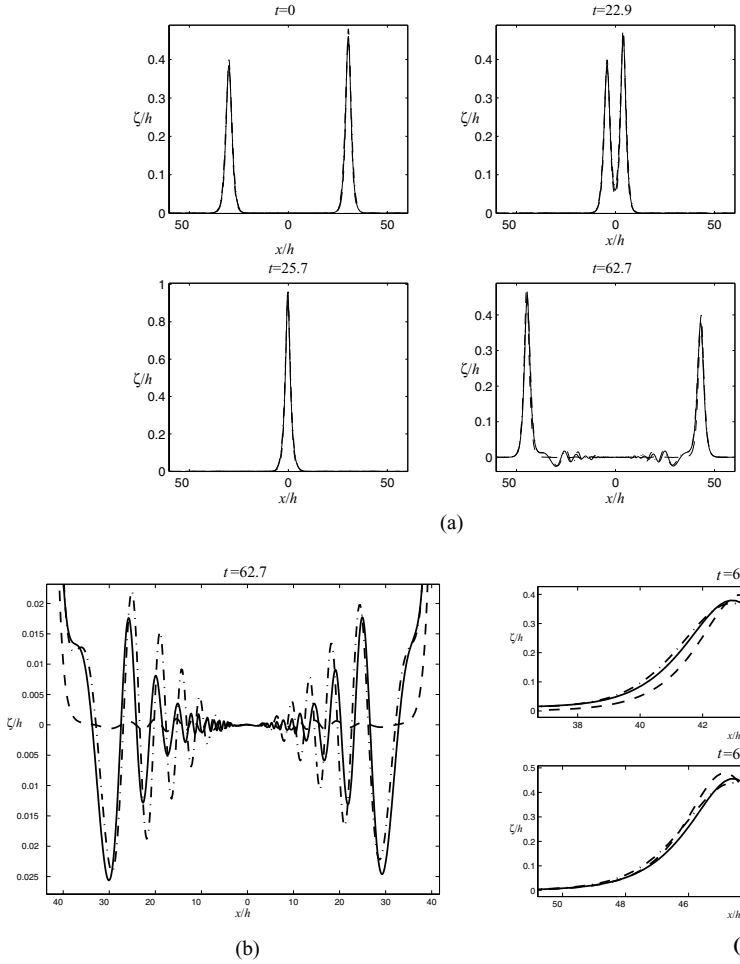

Figure 6. (a) The head-on collision of two solitary waves of the Euler (solid curve), the SG (dash-dotted curve), and Boussinesq equations (dashed curve), respectively, with the Froude numbers $F = 1.172$ and 1.201. (b) The trailing tails after the head-on collision. There is a noticeable difference between the exact solution and the Boussinesq solution in this highly nonlinear regime. (c) The wave profiles for $F = 1.172$ after the head-on collision. Notice that the head-on collisions of higher amplitude waves have a greater phase shift.

the collision is perfectly elastic) and the emerging solitary waves are almost identical to the incident waves.

In Figure 8, we show the overtaking collision of two solitary waves with a large amplitude ratio, which is about 7.8. The Froude numbers are $F = 1.172$ and 1.024 for large and small waves, respectively. In this case, the larger wave merges into the smaller wave to form a single peak during the interaction. The amplitude of the merged peak is, for example, about $a_{\mathrm{E}}/h = 0.3208$

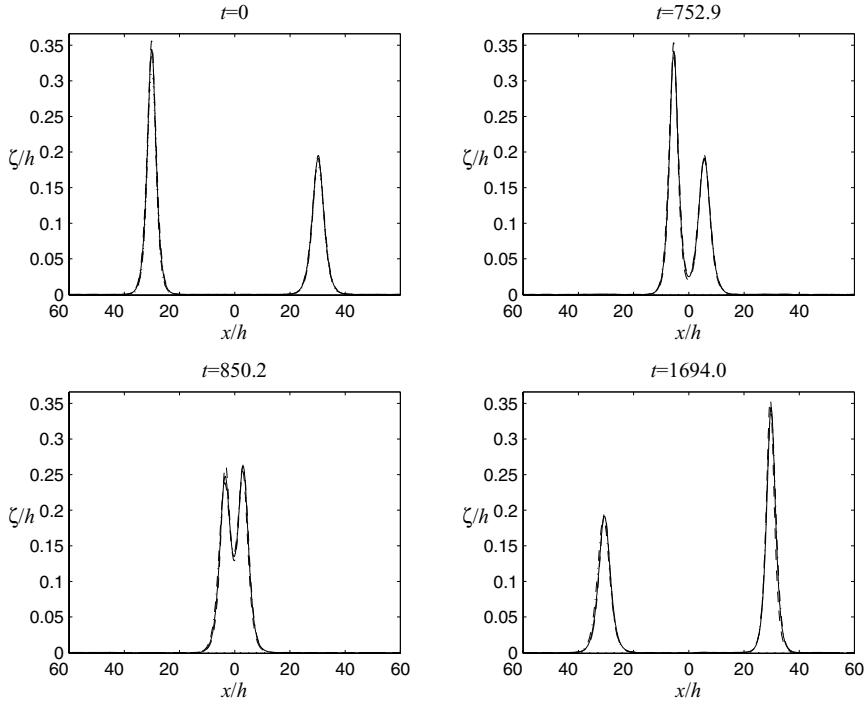

Figure 7. Overtaking collision of two solitary waves of the Euler (solid curve), SG (dash-dotted curve), Boussinesq (dashed curve), and KdV (dotted curve) equations, respectively, with $F = 1.156$ and 1.0904. The solutions are shown in a frame moving with $F = 1.123$. Unlike the case of head-on collision, the solitary waves of all the models emerge almost unchanged after an overtaking collision. This collision is perfectly elastic for the KdV equation.

for the Euler equations, which is smaller than the amplitude of the larger wave, $a_{\mathrm{E}}/h = 0.3847$. This is what the weakly nonlinear theory predicts. It is interesting to notice that, for the overtaking collision, the weakly nonlinear theory holds qualitatively even for large amplitude waves.

4.3. Disintegration of an initial elevation into solitary waves

In this section, we investigate the evolution of a single (Gaussian) elevation and compare numerical solutions of different models.

As shown in Figure 9(a), a single elevation of amplitude $a/h = 0.3$ quickly breaks into a higher wave of elevation traveling to the right and a smaller depression wave traveling to the left for the Euler equations, the SG equations, and the Boussinesq equations. For these bi-directional models, the relation between ζ and u for traveling solitary waves is used to fix u at $t = 0$. The wave of elevation traveling to the right further breaks into three solitary waves.

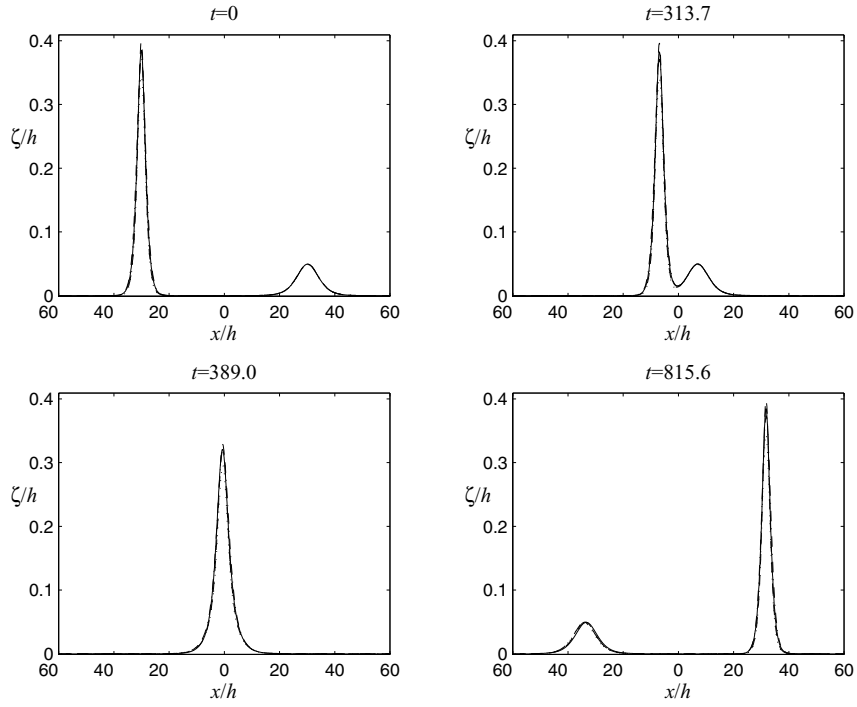

Figure 8. When a fast wave overtakes a slow wave, the slower wave is *swallowed* by the fast wave creating a single pulse wider and lower than the fast wave. The solutions of the Euler (solid curve), SG (dash-dotted curve), Boussinesq (dashed curve), and KdV (dotted curve) equations with the Froude numbers $F = 1.172$ and 1.024 are all in close agreement. The solutions are shown in a frame moving with $F = 1.098$. The larger wave overtakes the smaller wave to form a single peak. The amplitude of the merged peak for the Euler equations is smaller than the amplitude of the larger wave.

Although the (uni-directional) KdV equation does not shed off any small waves traveling to the left, the KdV solutions are similar to those of other models in terms of phase. As shown in Figure 9(b), the wave amplitude of the Boussinesq equations is always higher than those of the other three systems, while the KdV wave amplitude is always smaller than the others. The SG waves keep closer approximation to the Euler equations, in terms of wave amplitude, than weakly nonlinear systems. As we discussed previously, these results are consistent with the observation for solitary wave interactions.

Figure 10 shows the evolution of a single elevation of higher amplitude of $a/h = 0.57$ for the Euler equations, the SG equations, and the Boussinesq equations. The single wave splits into a higher wave of elevation moving to the right and a smaller elevation moving to the left. Afterwards, the larger wave moving to the right continues to shed small disturbances behind, all traveling

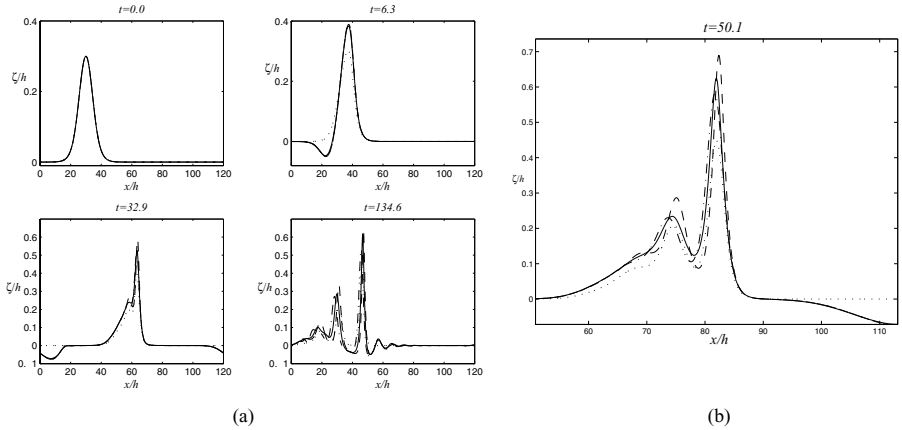

Figure 9. (a) Disintegration of a single elevation of amplitude 0.3 moving to the right: Euler (solid curve), SG (dash-dotted curve), Boussinesq (dashed curve), and KdV (dotted curve). (b) A closer observation of the process of breaking into three waves. The wave amplitude of the Boussinesq equations is always higher than those of other three systems, while the KdV wave amplitude is always smaller than others. The amplitude of the SG waves is closest to the Euler equations.

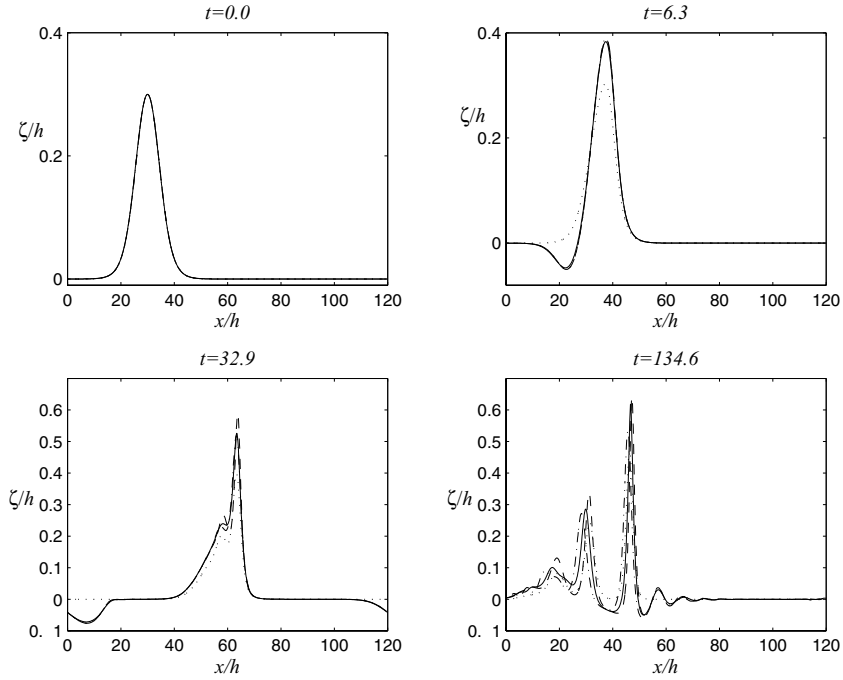

Figure 10. Disintegration of a single elevation of amplitude 0.57 moving to the right: Euler (solid curve), SG (dash-dotted curve), and Boussinesq (dashed curve). The single wave splits into a taller wave moving to the right and a shorter wave moving to the left. The right moving tall wave sheds small disturbances in its wake.

to the right. Similar to the previous case of the smaller wave amplitude, the Boussinesq waves are always slightly faster with larger amplitude, and the SG waves are slightly slower with smaller amplitude than others. We do not include the KdV solution because it does not approximate bi-directional waves, noticeably different from other solutions.

5. Conclusion

The full Euler equations are difficult to simulate when the wave interactions are highly nonlinear and the free surface constantly changes the domain boundary. We demonstrate the effectiveness of an efficient numerical method to solve a system of *exact* one-dimensional evolution equations for the motion of the free surface governed by the highly nonlinear Euler equations.

We solved two integral–partial differential evolution equations (7) derived from the Euler equations for the free surface elevation and the velocity potential on the parameterized free surface. These equations are derived by a time-dependent conformal mapping technique to map the fluid region of interest to a strip. The system is explicit and can be solved with the only slightly more effort than required to solve weakly nonlinear models such as the KdV, Boussinesq, or Su–Gardner equations. The approach has advantages over the boundary integral and other pseudo-spectral methods. The system is closed and no intermediate step, such as finding the strengths of singularities, is required. Also, Equations (7) were derived without assuming that the waves were small and the interactions were weakly nonlinear.

We demonstrated that the numerical method is robust and effective in simulating large amplitude long waves in water of finite depth. The maximum error in conserving mass, momentum, and energy was below 0.43% even in the long-time simulations (for example, $t = 1700$, as shown in Figure 7). Although we only considered the dynamics of solitary waves in this paper, the system given by (7) is useful to study periodic gravity–capillary waves of arbitrary wavelength.

Surprisingly, in terms of solitary wave dynamics, the weakly nonlinear models such as the Boussinesq equations and the KdV equation reasonably well-approximate steady solitary wave solutions of the Euler equations and their dynamics, even beyond the weakly nonlinear regime. The SG system seems to have a wider range of validity than weakly nonlinear asymptotic models, although the fully nonlinear Euler solutions are always necessary for the large amplitude waves. To make a more conclusive statement on the validity of the SG model, it is still necessary to investigate the behavior of the SG model for more realistic physical problems such as the dynamics of solitary waves over nonuniform bottom topography.

Acknowledgments

This work was supported by the DOE ASCR program under the Applied Mathematical Sciences Grant KJ010101. We would like to thank Roberto Camassa for his suggestions and Martin Staley for his helpful comments on numerical computations.

Appendix: Numerical methods for traveling waves

By using the KdV scaling, Friedrichs and Hyers [24] and Beale [25] proved the existence of solitary waves for the Euler equations in the weakly nonlinear regime where the Froude number $F = c/\sqrt{gh}$ is greater than but close to 1. They also showed that the KdV solitary waves approximate those of the Euler equations. Amick and Toland [26] showed the existence of solitary waves for the Euler equations as the limit of periodic waves even beyond the weakly nonlinear regime. Based on their results, we approximate the solitary waves of (7), or equivalently, the Euler equations, by long wavelength periodic waves.

We look for traveling waves of the form

$$x = \xi + \tilde{x}(\xi - ct), \quad y = y(\xi - ct),$$
$$\phi = \delta(\xi - ct) + \tilde{\phi}(\xi - ct), \quad \psi = \psi(\xi - ct),$$

where $\tilde{x}(=Ty)$, y, ψ, and $\tilde{\phi}$ are periodic functions of $s = \xi - ct$ with period l and δ which are constants to be determined. The functions y and $\tilde{\phi}$ satisfy the boundary conditions $y(l/2) = \tilde{\phi}_\xi(l/2) + \delta = 0$, and y is even and symmetric with respect to $s = 0$. As $l \to \infty$, $y(s)$ converges to a solitary wave decaying to zero [26].

Substituting the traveling wave into the kinematic equation $y_t x_\xi - x_t y_\xi = -\psi_\xi$ [8], we obtain $cy_s = \psi_s$. Because $\tilde{x}$ and ϕ are harmonic conjugates of y and ψ, respectively, we have that $\phi_s(s) = c(\tilde{x}_s(s) - \tilde{x}_s(l/2))$, i.e., $\delta = -c\tilde{x}_s(l/2)$. Substituting these relations into the third equation of (7) and assuming that the surface tension $\mathcal{S}$ and the external pressure $\mathcal{P}_E$ are negligible, the free surface equation can be reduced to

$$x_\xi^2 + y_\xi^2 = \frac{x_s^2(l/2)}{1 - 2gy/c^2}.$$

Substituting $s = \bar{h}\xi$, $x = \bar{h}\hat{x}$, and $y = \bar{h}\hat{y}$ into this equation leads to the dimensionless-free surface equation

$$\hat{x}_\xi^2 + \hat{y}_\xi^2 = \frac{\hat{x}_\xi^2(l/2)}{1 - 2g\bar{h}\hat{y}/c^2}. \tag{A.1}$$

Because the Euler equations have a one-parameter scaling symmetry group $(\lambda x, \lambda y, \lambda^{\frac{1}{2}} t, \lambda^{\frac{3}{2}} \phi)$ [13] for any $\lambda > 0$, without loss of generality, we set $\bar{h} = 1$ in the following analysis. Also, for simplicity, we will drop the accent $\hat{}$ over x and y .

Let w and θ be real-valued functions such that $z_\xi = x_\xi + i y_\xi = e^{w+i\theta}$. Because z_ξ is an analytic function of $\xi + i\eta$, w and θ satisfy the Cauchy–Riemann equations. Using the KdV scaling [24], $\xi^* = a\xi$, $\theta^* = a^{-3}\theta$, and $w^* = a^{-2}w$, the equation for the free surface given by (A.1) can be expressed as

$$w_\xi = \frac{1}{a^3} e^{a^2(3w - 2w(l/2) - 1)} \sin a^3\theta \quad \text{at } \eta = 0, \tag{A.2}$$

where $e^{a^2} = c^2/(g\bar{h})$ and we have dropped the asterisks for simplicity.

The exponent in (A.2) can be found using the Cauchy–Riemann relations as

$$3w - 2w(l/2) = 3T_a[\theta] - 2T_a[\theta(l/2)] + \langle w \rangle \equiv M_a[\theta], \tag{A.3}$$

where $T_a[\theta]$ is the scaled complex T-transform (4),

$$T_a[\theta] = -ia \sum_{k \neq 0} \coth(2\pi ak/l) c_k e^{2\pi i k\xi/l}.$$

Here $\langle w \rangle$ is the average value of w over one period,

$$\langle w \rangle = -\frac{1}{a^2} \log \left[\frac{1}{l} \int_0^l e^{a^2 T_a \theta} \cos(a^3\theta)\, d\xi \right].$$

By using (A.3), Equation (A.2) can be written as

$$f[\theta] \equiv \theta - (G[\theta] - I)^{-1} \left[\frac{1}{a^3} e^{a^2(M_a[\theta] - 1)} \sin(a^3\theta) - \theta \right] = 0, \tag{A.4}$$

where

$$G[\theta] \stackrel{\text{def}}{=} a \sum_{k \neq 0} kl \coth(2\pi ak/l) c_k e^{2\pi i k\xi/l}.$$

To solve (A.4) with the Newton's method, we express the $(n + 1)$st approximation to θ as $\theta_{n+1} = \theta_n + v_n$, where θ_n is the approximation from the previous iteration and v_n is the correction. We then linearize (A.4) with respect to v_n to obtain $f_{\theta_n}[v_n] = -f[\theta_n]$. Here f_θ is the functional derivative of f with respect to θ

$$f_{\theta_n}[v_n] \equiv v_n - (G - I)^{-1} \times \left[\frac{1}{a} e^{a^2(M_a[\theta_n] - 1)} \sin\left(a^3\theta_n\right) \frac{\delta M_a}{\delta \theta_n} + e^{a^2(M_a[\theta_n] - 1)} \cos\left(a^3\theta_n\right) - 1 \right] v_n.$$

After we compute f_θ, we define the $N \times N$ matrix, F_θ, as f_θ modulus its kernel using the discrete Fourier Transform for N Fourier modes. We then solve $F_{\theta_n}[v_n] = -f[\theta_n]$ for v_n and iterate until $|v_n| < 10^{-13}$.

Because small-amplitude waves of the KdV equation are close approximations to those of the Euler equations [24, 25], in the weakly nonlinear regime (small $a > 0$), we use the KdV traveling waves as the initial guess to find traveling wave solutions of (A.2). We then gradually increase the parameter a (thus, increasing the speed c), and use solutions for the smaller waves as an initial guess to compute higher amplitude waves as the solution of a fixed-point problem. In the weakly nonlinear regime, if we increase a by 7%, it takes only six iterations for this scheme to reduce the error to $\sup|\theta_{n+1} - \theta_n| < 10^{-13}$ and $\sup|f[\theta_n]| < 10^{-13}$.

References

1. W. Tsai and D. K. P. Yue, Computation of nonlinear free-surface flows, *Ann. Rev. Fluid Mech.* 28:249–278 (1996).
2. J. D. Fenton and M. M. Rienecker, A Fourier method for solving nonlinear water-wave problems: Application to solitary-wave interactions, *J. Fluid Mech.* 118:411–443 (1982).
3. D. G. Dommermuth and D. K. P. Yue, A higher-order spectral method for the study of nonlinear gravity waves, *J. Fluid Mech.* 184:267–288 (1987).
4. W. Craig and C. Sulem, Numerical simulation of gravity waves, *J. Comput. Phys.* 108:73–83 (1993).
5. M. S. Longuet-Higgins and E. D. Cokelet, The deformation of steep surface waves on water I. A numerical method of computation, *Proc. R. Soc. Lond. A* 350:1–26 (1976).
6. L. V. Ovsjannikov, To the shallow water theory foundation, *Arch. Mech.* 26:407–422 (1974).
7. A. L. Dyachenko, V. E. Zakharov, and E. A. Kuznetsov, Nonlinear dynamics of the free surface of an ideal fluid, *Plasma Phys. Rep.* 22:916–928 (1996).
8. W. Choi and R. Camassa, Exact evolution equations for surface waves, *J. Eng. Mech.* 125:756–760 (1999).
9. W. Choi, Nonlinear evolution equation for two-dimensional surface waves in a fluid of finite depth, *J. Fluid Mech.* 295:381–394 (1995).
10. D. J. Korteweg and G. de Vries, On the change of form of long waves advancing in a rectangular canal, and on a new type of long stationary waves, *Philos. Mag.* 39:422–443 (1895).
11. J. Boussinesq, Essai sur la théorie des eaux courants, *Mem. Prés. Div. Sav. Acad. Sci. Inst. Fr.* 23:1–680 (1877).
12. C. H. Su and C. S. Gardner, Korteweg–de Vries equation and generalizations. III: Derivation of the Korteweg–de Vries equation and Burgers equation, *J. Math. Phys.* 10:536–539 (1969).
13. T. B. Benjamin and P. J. Olver, Hamiltonian structure, symmetries and conservation laws for water waves, *J. Fluid Mech.* 125:137–185 (1982).
14. A. E. Green and P. M. Naghdi, Derivation of equations for wave propagation in water of variable depth, *J. Fluid Mech.* 78:237–246 (1976).
15. G. B. Whitham, *Linear and Nonlinear Waves*, Wiley, New York, 1974.
16. G. Wei, J. T. Kirby, S. T. Grilli, and R. Subramanya, A fully nonlinear Boussinesq model for surface waves. 1. Highly nonlinear unsteady waves, *J. Fluid Mech.* 294:71–92 (1995).

17. M. S. Longuet-Higgins, On the mass, momentum, energy and circulation of a solitary wave, *Proc. R. Soc. Lond. A* 337:1–13 (1974).
18. M. S. Longuet-Higgins and J. D. Fenton, On the mass, momentum, energy and circulation of a solitary wave. II, *Proc. R. Soc. Lond. A* 340:471–493 (1974).
19. T. Maxworthy, Experiments on collisions between solitary waves, *J. Fluid Mech.* 76:177–185 (1976).
20. C. H. Su and R. M. Mirie, On head-on collisions between 2 solitary waves, *J. Fluid Mech.* 98:509–525 (1980).
21. C. H. Su and R. M. Mirie, Collisions between 2 solitary waves. 2. A numerical study, *J. Fluid Mech.* 115:475–492 (1982).
22. Q. S. Zou and C. H. Su, Overtaking collision between 2 solitary waves, *Phys. Fluids* 29:2113–2123 (1986).
23. T. Y. Wu, Bidirectional soliton street, *Acta Mech. Sinica* 11:289–306 (1995).
24. K. O. Friedrichs and D. H. Hyers, The existence of solitary waves, *Comm. Pure Appl. Math.* 7:517–550 (1954).
25. T. Beale, The existence of solitary waves, *Comm. Pure Appl. Math.* 30:373–389 (1977).
26. C. J. Amick and J. F. Toland, On periodic water-waves and their convergence to solitary waves in the long-wave limit, *Phil. Trans. Roy. Soc. Lond. A* 303:633–669 (1981).

Stevens Institute of Technology
Los Alamos National Laboratories
University of Michigan

(Received March 8, 2004)